Synthesis and Characterization of a Series of Edge-Sharing Octahedral−Tetrahedral−Octahedral Linear Trinuclear Complexes $[M_3(L1O)_4]^{2+}$, Where M = Mn^{2+}, Co^{2+}, Ni^{2+}, Cu^{2+}, and Zn^{2+} and L1OH Is the "Heteroscorpionate" Ligand (2-Hydroxyphenyl)bis(pyrazolyl)methane

Timothy C. Higgs,[†] K. Spartalian,[‡] Charles J. O'Connor,[§] Berthold F. Matzanke,[||] and Carl J. Carrano*,[†]

Departments of Chemistry, Southwest Texas State University, San Marcos, Texas 78666, and University of New Orleans, New Orleans, Louisiana 70148, Department of Physics, University of Vermont, Burlington, Vermont 05405, and The Institute for Physics, Medical University of Lübeck, D-23538 Lübeck, Germany

Received July 7, 1997

The mixed functionality pyrazole/phenol ligand (2-hydroxyphenyl)bis(pyrazolyl)methane, L1OH, has been used to prepare a series of linear trimetallic systems with the general structural motif $[M_3(L1O)_4]^{2+}$, where M = Mn^{2+}, Co^{2+}, Ni^{2+}, Cu^{2+}, and Zn^{2+}. Each of these complexes has been structurally characterized by X-ray crystallography giving the following structural parameters: $[Zn_3(L1O)_4][BF_4]_2 \cdot H_2O$, $C_{52}H_{44}N_{16}B_2F_8O_5Zn_3$, monoclinic, a = 18.572(4) Å, b = 22.400(5) Å, c = 15.921(3), β = 112.439(8)°, space group $C2/c$, Z = 4; $[Cu_3(L1O)_4][BF_4]_2 \cdot 2MeCN$, $C_{56}H_{44}N_{18}B_2Cu_3F_8O_4$, monoclinic, a = 40.574(2) Å, b = 16.701(1) Å, c = 19.841(2) Å, β = 111.388(5)°, space group $C2/c$, Z = 8; $[Ni_3(L1O)_4][ClO_4]_2 \cdot MeCN \cdot 0.5H_2O$, $C_{54}H_{44}N_{17}Cl_2Ni_3O_{12.5}$, monoclinic, a = 12.324(4) Å, b = 26.537(2) Å, c = 18.829(3) Å, β = 102.78(1)°, space group $C2/c$, Z = 4; $[Co_3(L1O)_4][BF_4]_2 \cdot MeCN$, $C_{54}H_{44}N_{17}B_2Co_3F_8O_4$, monoclinic, a = 12.395(2) Å, b = 26.483(3) Å, c = 18.703(4) Å, β = 103.22(2)°, space group $C2/c$, Z = 4; $[Mn_3(L1O)_4(MeCN)][ClO_4]_2 \cdot 1.4MeCN$, $C_{56.68}H_{44}N_{18.34}Cl_2Mn_3O_{12}$, orthorhombic, a = 15.471(2) Å, b = 17.364(2) Å, c = 24.216(2) Å, space group $Pbcn$, Z = 4. For Zn^{2+}, Cu^{2+}, Ni^{2+}, and Co^{2+} the central metal atom of the linear trimetallic $[M_3(L1O)_4]^{2+}$ unit is four coordinate and has a pseudotetrahedral geometry with a dihedral angle, ω, between the two $M_{central}O_2M_{terminal}$ planes of 79.9° (Zn), 61.2° (Co), 60.4° (Ni), and 46.8° (Cu). The central Mn^{2+} atom of $[Mn_3(L1O)_4(MeCN)][ClO_4]_2 \cdot 1.4MeCN$ is five-coordinate, with a trigonal bipyramidal stereochemistry, the result of an equatorially coordinated MeCN solvent molecule. Variable-temperature magnetic data indicate that the Ni, Cu, and Mn complexes display modest antiferromagnetic coupling between the metal centers, while the Co derivative is strongly ferromagnetically coupled.

Introduction

We have previously described the synthesis and some of the coordination properties of a new class of heteroscorpionate ligands.[1−3] These ligands are of the general type L_2CX, where L = 3(5)-substituted pyrazole and X = functionalized donor, i.e., a substituted phenol or thiophenol. We have shown that the nature of the metal complex formed by these ligands depends on the particular metal involved and the degree of substitution on both the phenyl and pyrazole arms, as well as the ligand-to-metal ratio. By varying the metal:ligand ratio, we show here that it is possible to prepare a series of homometallic, linear, trinuclear species where, due to the basicity of the coordinated phenols, an octahedral metal complex functions as a bidentate ligand for a tetrahedrally coordinated central metal. These edge-sharing octahedral−tetrahedral−octahedral species nicely complement the elegant studies of the face sharing all octahedral trinuclear species reported by Wieghardt and co-workers.[4−6] Indeed the homometallic linear trimeric $[(L1O)_2MMM(L1O)_2]^{2+}$ cations of the paramagnetic Cu^{2+}, Ni^{2+}, and Co^{2+} metal ions afford an excellent opportunity to investigate the effect of changing the metal atom within a fixed ligand and structural framework.[7] Thus, it should be possible to identify how electronic factors influence the magnitude of any spin−spin interactions. Any interactions could be considerably different from those observed in the trimeric (Ni^{2+}, Co^{2+}) compounds of Wieghardt et al.[4−6] since the magnetic orbitals involved in any potential spin−spin interaction will be different due to the contrasting octahedral/octahedral/octahedral versus octahedral/tetrahedral/octahedral motifs present in these two sets of compounds.

Experimental Section

All operations were carried out in air unless otherwise stated, and the solvents used were of reagent grade (Aldrich Chemical Co.).

[†] Southwest Texas State University.
[‡] University of Vermont.
[§] University of New Orleans.
[||] Medical University of Lubeck.

(1) Higgs, T. C.; Carrano, C. J. *Inorg. Chem.* **1997**, *36*, 291.
(2) Higgs, T. C.; Carrano, C. J. *Inorg. Chem.* **1997**, *36*, 298.
(3) Higgs, T. C.; Ji, D.; Czernuscewicz, R. S.; Carrano, C. J. *Inorg. Chim. Acta* **1998**, in press.
(4) Auerbach, U.; Stockheim, C.; Weyhermuller, T.; Wieghardt, K.; Nuber, B. *Angew. Chem., Int. Ed. Engl.* **1993**, *32*, 714.
(5) Beissel, T.; Glaser, T.; Kesting, F.; Wieghardt, K.; Nuber, B. *Inorg. Chem*. **1996**, *35*, 3936.
(6) Beissel, T.; Birkelbach, F.; Bill, E.; Glaser, T.; Kesting, F.; Krebs, C.; Weyhermuller, T.; Wieghardt, K.; Butzlaff, C.; Trautwein, A. X. *J. Am. Chem. Soc*. **1996**, *118*, 12376. Ginsberg, A. P.; Martin, R. L.; Sherwood, R. C. *Inorg. Chem*. **1968**, *7*, 932.
(7) Kahn, O. *Molecular Magnetism*; VCH Publishers: Weinheim, Germany, 1993.

S0020-1669(97)00844-6 CCC: $15.00
Published on Web 04/14/1998

Anhydrous THF was dried over Na/benzophenone. Microanalyses were performed by Desert Analytics Laboratory, Tucson, AZ. IR spectra were recorded as KBr disks on a Perkin-Elmer 1600 Series FTIR. Solution electronic spectra were obtained using a Hewlett-Packard 8452A diode array spectrophotometer under the computer control of a Compaq Deskpro 386S with OLIS diode array spectrophotometry software (On-line Instruments Inc.). Variable-temperature magnetic data were recorded over the range 2−300 K in a 1.0 T external field using a SQUID magnetometer as previously described.[8] Data were corrected for underlying diamagnetism and temperature-independent paramagnetism (TIP). The diamagnetic correction utilized Pascal's constants, while TIP was a fitted parameter in subsequent simulations. EPR spectra were recorded on a Bruker ESP 300e spectrometer equipped with an ESR 910 helium cryostat (Oxford Instruments).

Synthesis. The ligand L1OH was synthesized as previously described.[2] The sodium salt was prepared by taking the free ligand (2.00 g, 8.33 mmol) dissolved in anhydrous THF (25 cm^3) under argon and adding solid 95% NaH (0.35 g, 14.6 mmol). The reaction mixture was stirred at room temperature for 1 h, during which time evolution of hydrogen gas was observed. The excess NaH was then carefully filtered off (in air) and destroyed. The yellow filtrate was evaporated to dryness. The product was dissolved in Et_2O (20 cm^3) to which hexane (80 cm^3) was added causing the instant precipitation of a dense white microcrystalline solid. This solid was collected by filtration, washed with hexane (20 cm^3), and dried in vacuo. Yield: 2.14 g (97%).

$[Zn_3(L1O)_4][BF_4]_2 \cdot 2H_2O$, 1. L1OH (0.20 g, 0.83 mmol) was dissolved in MeOH (10 cm^3) forming a colorless solution. To this solution was added NaOMe (0.045 g, 0.83 mmol) which quickly dissolved. $Zn(BF_4)_2 \cdot 6H_2O$ (0.152 g, 0.416 mmol) was added to the solution which initially rapidly dissolved but was followed by the precipitation of a microcrystalline white solid. The mixture was stirred for 30 min at room temperature before the solid was collected by filtration, washed with MeOH (5 cm^3), and dried in vacuo. Yield: 0.14 g (74%). Anal. Calcd for $C_{52}H_{48}N_{16}B_2F_8O_6Zn_3$: C, 45.82; H, 3.52; N, 16.45. Found: C, 45.89; H, 3.24; N, 16.38.

$[Cu_3(L1O)_4][BF_4]_2$, 2. NaL1O (0.20 g, 0.763 mmol) was dissolved in MeOH (10 cm^3) forming a colorless solution. To this solution was added $Cu(BF_4)_2 \cdot 6H_2O$ (0.102 g, 0.305 mmol) which quickly dissolved to form a dark brown solution which gradually turned an intense crimson-red. The reaction mixture was stirred for 30 min at room temperature, during which time a dark red microcrystalline solid precipitated out of the solution. The solid was collected by filtration, washed with MeOH (2 cm^3) and Et_2O (5 cm^3), and dried in vacuo. Yield: 0.088 g (60%). Anal. Calcd for $C_{52}H_{44}N_{16}B_2Cu_3F_8O_4 \cdot 3H_2O$: C, 45.43; H, 3.64; N, 16.29. Found: C, 44.96; H, 2.93; N, 15.66.

$[Ni_3(L1O)_4][ClO_4]_2 \cdot H_2O$, 3. $Ni(ClO_4)_2 \cdot 6H_2O$ (0.457 g, 1.25 mmol) was dissolved in MeOH (5 cm^3) forming a pale green solution. Separately, L1OH (0.20 g, 0.833 mmol) was dissolved in MeOH (10 cm^3), and to this solution was added NaOMe (0.045 g, 0.833 mmol). The NaL1O solution was then added to the solution of $Ni(ClO_4)_2 \cdot 6H_2O$, the color of which became more intense and changed hue slightly. The mixture was stirred for 20 h at room temperature, during which time a pale brown microcrystalline solid was deposited from the reaction mixture. The solid was collected by filtration, washed with MeOH (2 cm^3), and dried in vacuo. Yield: 0.12 g (43%). Anal. Calcd for $C_{52}H_{46}N_{16}Cl_2Ni_3O_{13}$: C, 46.32; H, 3.41; N, 16.63. Found: C, 46.24; H, 3.15; N, 16.58.

$[Co_3(L1O)_4][BF_4]_2 \cdot 2H_2O$, 4. L1OH (0.20 g, 0.833 mmol) was dissolved in MeOH (10 cm^3), and to this solution was added NaOMe (0.045 g, 0.833 mmol). Separately, $Co(BF_4)_2 \cdot 6H_2O$ (0.426 g, 1.25 mmol) was dissolved in MeOH (5 cm^3), forming a pale purple/red solution. The two solutions were then mixed together resulting in the formation of a purple solution followed by the rapid precipitation of a purple microcrystalline solid. This solid was collected by filtration, washed with MeOH (2 cm^3), Et_2O (5 cm^3), and dried in vacuo. Yield: 0.17 g (61%). Anal. Calcd for $C_{52}H_{48}N_{16}B_2Co_3F_8O_6$: C, 46.48; H, 3.57; N, 16.69. Found: C, 46.35; H, 3.15; N, 16.57.

$[Mn_3(L1O)_4(MeCN)][ClO_4]_2 \cdot H_2O$, 5. L1OH (0.20 g, 0.833 mmol) was dissolved in MeOH (10 cm^3), and NaOMe (0.045 g, 0.833 mmol) was added to the solution. $Mn(ClO_4)_2 \cdot 6H_2O$ (0.302 g, 0.833 mmol) was then added, and it quickly dissolved causing the solution color to change from colorless to brown. The reaction mixture was stirred for 30 min at room temperature, during which time a white microcrystalline precipitate had formed in the solution. The solid was collected by filtration, washed with MeOH (4 cm^3), and dried in vacuo. The resultant white microcrystalline solid was dissolved in MeCN (5 cm^3), and the solution was transferred to a boiling tube and layered with diisopropyl ether (25 cm^3). The tube was sealed and over a period of several days large blocklike, very pale brown crystals of the product formed. The crystals were collected by filtration and dried in vacuo. Yield: 0.16 g (56%). Anal. Calcd for $C_{54}H_{49}N_{17}Cl_2Mn_3O_{13}$: C, 47.00; H, 3.55; N, 17.26. Found: C, 47.30; H, 3.61; N, 16.89.

Crystallography. X-ray-quality crystals of all the complexes were grown by layering a MeCN solution of the compound with isopropyl ether. For each structure determination the crystals were sealed in thin-walled quartz capillary tubes to prevent loss of lattice solvent to which all were prone. The crystals were mounted on a Siemens P4 diffractometer with a sealed tube Mo Kα X-ray source ($\lambda = 0.710\ 73$ Å) under computer control with installed Siemens XSCANS 2.20 software. Automatic searching, centering, indexing, and least-squares routines were carried out for each crystal with 20−25 relatively high-angle reflections used to determine unit cell parameters. During the data collections, the intensities of three representative reflections were measured every 97 reflections, and any decay (presumably from loss of lattice solvent) was corrected for. The data were also corrected for Lorentz and polarization effects and for $[Zn_3(L1O)_4][BF_4]_2 \cdot H_2O$ and $[Co_3(L1O)_4][BF_4]_2 \cdot MeCN$ for crystal absorption using a semiempirical correction determined from ψ-scan data. Structure solutions were obtained by direct methods or via the Patterson function and refinement by difference Fourier synthesis was accomplished using the Siemens SHELXTL PC software package.[9] A summary of cell parameters, data collection conditions, and refinement results is given in Table 1. Summary bond lengths and angles are given in Tables 2−6. Details pertinent to the individual determinations follow:

The structure of $[Zn_3(L1O)_4][BF_4]_2 \cdot H_2O$ was solved, with difficulty due to pseudosymmetry problems, by direct methods. After correct location of the three zinc atoms subsequent location of the lighter atoms was accomplished by additional cycles of least-squares refinement, initially isotropic and then anisotropic. The asymmetric unit contains half a $[Zn_3(L1O)_4]^{2+}$ cation as well as one $[BF_4]^-$ anion and two lattice water molecules at 0.25 occupancy. Hydrogen atoms were included in calculated positions using a riding model and fixed isotropic thermal parameters, with the exception of lattice water molecules for which hydrogen atoms were neither located nor calculated.

The structure of $[Cu_3(L1O)_4][BF_4]_2 \cdot 2MeCN$ was again solved by direct methods, the asymmetric unit containing one $[Cu_3(L1O)_4]^{2+}$ cation and two $[BF_4]^-$ anions, one of which was disordered. The disordered $[BF_4]^-$ group had one fluorine atom disordered over two positions (F1 and F1A); the occupancies of these two positions were tied to equal 1.0, and their respective occupancies were then refined yielding a value of 0.61 for F1 and 0.39 for F1A. Isotropic refinement additionally revealed the presence of two molecules of lattice MeCN in the asymmetric unit, both at full occupancy. All the non-hydrogen atoms were anisotropically refined except for the lower occupancy fluorine atom (F1A) of the disordered $[BF_4]^-$ group. The hydrogen atom positions were calculated and included in the final cycles of refinements using a riding model with fixed isotropic thermal parameters with the exception of the two lattice MeCN molecules for which no hydrogen atoms were included in the structure factor calculation.

The structure of $[Ni_3(L1O)_4][ClO_4]_2 \cdot MeCN \cdot 0.5H_2O$ was solved by use of the Patterson function, which indicated that the asymmetric unit contains half of a $[Ni_3(L1O)_4]^{2+}$ cation. The asymmetric unit also contains one disordered $[ClO_4]^-$ anion with one of its oxygen atoms disordered over two positions, both at 0.5 occupancy. Subsequent isotropic refinement also located a lattice MeCN molecule at 0.5

(8) O'Connor, C. J. *Prog. Inorg. Chem.* **1982**, *29*, 203.
(9) Sheldrick, G. M. *SHELXTL-PC*, version 4.1; Siemens X-ray Analytical Instruments, Inc.: Madison, WI, 1989.

Table 1. Crystallographic Data and Data Collection Parameters for $[Zn_3(L1O)_4][BF_4]_2 \cdot H_2O$, $[Cu_3(L1O)_4][BF_4]_2 \cdot 2MeCN$, $[Ni_3(L1O)_4][ClO_4]_2 \cdot MeCN \cdot 0.5H_2O$, $[Co_3(L1O)_4][BF_4]_2 \cdot MeCN$, and $[Mn_3(L1O)_4(MeCN)][ClO_4]_2 \cdot 1.4MeCN$

	compound				
param	$[Zn_3(L1O)_4][BF_4]_2$	$[Cu_3(L1O_4][BF_4]_2$	$[Ni_3(L1O)_4][ClO_4]_2$	$[Co_3(L1O)_4][BF_4]_2$	$[Mn_3(L1O)_4(MeCN)][ClO_4]_2$
formula	$C_{52}H_{44}N_{16}B_2F_8O_5Zn_3$	$C_{56}H_{44}N_8B_2Cu_3F_8O_4$	$C_{54}H_{44}N_{17}Cl_2Ni_3O_{12.5}$	$C_{54}H_{44}N_{17}B_2Co_3F_8O_4$	$C_{56.68}H_{44}N_{18.34}Cl_2Mn_3O_{12}$
space group	*C*2/*c*	*C*2/*c*	*C*2/*c*	*C*2/*c*	*Pbcn*
a, Å	18.572(4)	40.574(2)	12.324(4)	112.395(2)	15.471(2)
b, Å	22.400(5)	16.701(1)	26.537(2)	26.483(3)	17.364(2)
c, Å	15.921(3)	19.841(2)	18.829(3)	18.703(4)	24.216(2)
α, deg	90.003(9)	89.983(6)	89.942(8)	90.04(1)	90.03(1)
β, deg	112.439(8)	111.388(5)	102.78(1)	103.22(2)	90.005(8)
γ, deg	90.01(1)	90.012(5)	89.95(2)	89.996(6)	90.001(9)
V, Å^3	6121.8(35)	12518.9(17)	6005.4(15)	5977.1(21)	6505.5(12)
ρ, g cm^{-3}	1.455	1.483	1.524	1.495	1.440
Z	4	8	4	4	4
fw	1340.7	1397.3	1378.1	1345.5	1409.7
cryst size, mm	0.6 × 0.6 × 0.4	0.6 × 0.6 × 0.15	0.5 × 0.4 × 0.2	0.6 × 0.4 × 0.2	0.7 × 0.5 × 0.3
cryst color, habit	colorless, block	dark brown, plate	brown, block	red/purple, block	colorless, block
μ, mm^{-1}	1.248	1.094	1.096	0.908	0.729
no. unique data	3866	8064	3874	3875	3818
no. obsd data	1929 ($F > 5\sigma(F)$)	4363 ($F > 4\sigma(F)$)	2031 ($F > 4\sigma(F)$)	2521 ($F > 5\sigma(F)$)	2236 ($F > 5\sigma(F)$)
data:param ratio	4.8:1	5.4:1	4.8:1	5.1:1	5.2:1
transm factors	0.7606/0.9641			0.7486/0.7843	
R^a	5.36	6.21	5.28	4.64	6.82
$R_w{}^a$	6.63	6.82	5.51	5.62	8.28
max diff peak, e Å^{-3}	−0.50	+0.77	−0.37	+0.57	+0.54
Δ/*σ*(mean)	0.001	0.033	0.012	0.017	0.078

[a] Quantity minimized $\omega w(F_o - F_c)^2$. $R = \sum|F_o - F_c|/\omega F_o$. $R_w = (\omega w(F_o - F_c)^2/\sum(\omega F_o)^2)^{1/2}$. Data collection range, 3.5−45.0°; radiation, Mo Kα; temperature, 298 K; scan type, $\theta-2\theta$.

occupancy and a lattice water molecule at 0.25 occupancy. All non-hydrogen atoms were refined anisotropically with the exception of the lattice water molecule. Hydrogen atoms were included in calculated positions using a riding model and fixed isotropic thermal parameters with the exception of the lattice solvent molecules.

For $[Co_3(L1O)_4][BF_4]_2 \cdot MeCN$ structure solution was achieved via the Patterson function with the asymmetric unit containing half of a linear trimeric $[Co_3(L1O)_4]^{2+}$ cation and a disordered $[BF_4]^-$ anion with one fluorine atom disordered over two positions (at 0.7 and 0.3 occupancies). Subsequent, isotropic refinement located a lattice MeCN molecule at 0.5 occupancy. All the non-hydrogen atoms were refined anisotropically. The hydrogen atoms were located by difference Fourier synthesis and were refined isotropically.

Solution of the structure of $[Mn_3(L1O)_4(MeCN)][ClO_4]_2 \cdot 1.4MeCN$ by direct methods revealed half of a $[Mn_3(L1O)_4(MeCN)]^{2+}$ cation, the other half being generated by a 2-fold rotation about a crystallographic C_2 axis. Additionally a disordered $[ClO_4]^-$ was located in the asymmetric unit with one oxygen atom disordered over two positions, one at 0.6 and the other at 0.4 occupancy. Isotropic refinement located a lattice MeCN molecule, the occupancy of which was refined to 0.7. All non-hydrogen atoms were refined anisotropically with the exception of the lower occupancy (0.4) oxygen atom of the disordered $[ClO_4]^-$ group. The hydrogen atoms were included in calculated positions using a riding model with fixed isotropic thermal parameters with the exception of the lattice MeCN molecule whose hydrogen atoms were not included in the calculation.

Results

Description of Structures. The crystal structure of complex **1** consists of asymmetric units containing half of a linear trimeric $[Zn_3(L1O)_4]^{2+}$ cation, one $[BF_4]^-$ anion, and four water molecules at 0.25 occupancy (Figure 1). The linear trimeric $[Zn_3(L1O)_4]^{2+}$ cation has the three Zn^{2+} atoms positioned on the crystallographic 2-fold rotation axis. It has two terminal Zn^{2+} atoms which are 6-coordinated by two $[L1O]^-$ ligands in a tripodal, tridentate fashion. For each terminal Zn^{2+} the two coordinated $[L1O]^-$ ligands are in a cis orientation with respect to the phenolate oxygen atom donors which bridge to another (the central) Zn^{2+} atom forming the linear trimeric moiety. The central metal atom, Zn1, thus possesses O_4-ligated 4-coordination, the dihedral angle between the two $Zn_{terminal}O_2Zn_{central}$ planes of 79.9° being close to the value for an "ideal" tetrahedral geometry (90°). The individual O−Zn−O angles show considerable distortion from "ideal" tetrahedral values (109.5°), however, with O1−Zn1−O1A and O2−Zn1−O2A (83.4(5) and 83.5(4)°, respectively) being highly compressed due to formation of the four-membered $Zn_{terminal}O_2Zn_{central}$ chelate ring which in turn results in a corresponding expansion of the other O−Zn−O angles (Table 2). The geometries of the terminal, 6-coordinate Zn^{2+} atoms are distorted octahedral, the most distorted angles are the cis O−Zn−O angles (average, 77.0°). These angles being compressed by the formation of the $Zn_{central}O_2Zn_{terminal}$ four-membered chelate rings. The Zn−O bond distances for the central metal atom (average, 1.956 Å) are smaller than the corresponding bond lengths for the terminal metal atoms (average, 2.123 Å). This difference is attributable to the difference in stereochemistry between the central and terminal Zn^{2+} atoms (tetrahedral versus octahedral). The Zn1−O1−Zn3 and Zn1−O2−Zn2 bond angles of 99.7(4) and 99.9(3)°,

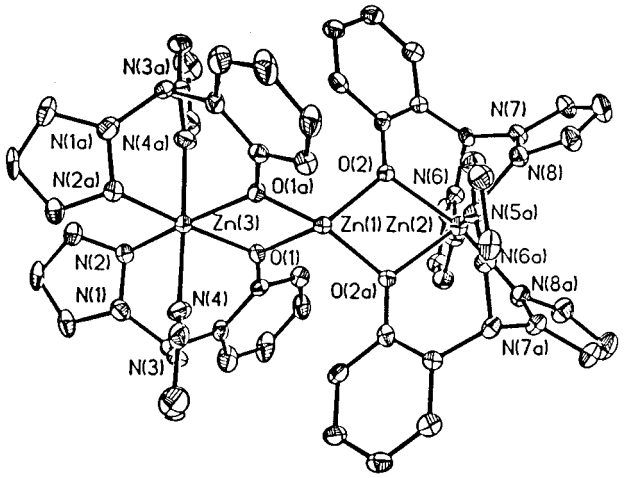

Figure 1. ORTEP diagram showing 30% probability ellipsoids and partial atomic labeling of **1**.

Table 2. Bond Distances (Å) and Angles (deg) for $[Zn_3(L1O)_4][BF_4]_2 \cdot H_2O$

	Zn2 Bond Distances		
Zn2−O2	2.095(7)	Zn2−N5	2.102(11)
Zn2−N8	2.125(10)	Zn2−O2A	2.095(7)
Zn2−N5A	2.102(11)	Zn2−N8A	2.125(10)
	Zn2 Angles		
O2−Zn2−N5	83.3(3)	O2−Zn2−N8	92.9(3)
N5−Zn2−O2A	101.5(4)	N5−Zn2−N5A	174.0(5)
O2A-Zn2−N5A	83.3(3)	O2−Zn2−N8A	165.4(4)
N8−Zn2−N8A	99.0(5)	N5A-Zn2−N8A	87.4(4)
N5−Zn2−N8	87.4(4)	O2−Zn2−O2A	76.8(4)
N8−Zn2−O2A	165.4(4)	O2−Zn2−N5A	101.5(4)
N8−Zn2−N5A	88.7(4)	N5−Zn2−N8A	88.7(4)
O2A-Zn2−N8A	92.9(3)		
	Zn3 Bond Distances		
Zn3−N2	2.153(12)	Zn3−O1	2.088(8)
Zn3−O1A	2.088(8)	Zn3−N4	2.110(9)
Zn3−N4A	2.110(9)	Zn3−N2A	2.153(12)
	Zn3 Angles		
O1−Zn3−N2	93.6(4)	N2−Zn3−N4	86.8(4)
O1−Zn3−N4	84.6(4)	O1−Zn3−O1A	77.2(5)
N2−Zn3−O1A	169.8(4)	N4−Zn3−O1A	96.6(4)
N2−Zn3−N2A	95.8(6)	O1−Zn3−N2A	169.8(4)
O1A-Zn3−N2A	93.6(4)	N4−Zn3−N2A	92.2(4)
O1−Zn3−N4A	96.6(4)	N2−Zn3−N4A	92.2(4)
N4−Zn3−N4A	178.5(6)	O1A-Zn3−N4A	84.6(4)
N2A-Zn3−N4A	86.8(4)		
	Zn1 Bond Distances		
Zn1−O1	1.959(8)	Zn1−O2A	1.953(7)
Zn1−O2	1.953(7)	Zn1−O1A	1.959(8)
	Zn1 Angles		
O2−Zn1−O1	129.4(3)	O2−Zn1−O2A	83.5(4)
O1−Zn1−O2A	118.7(3)	O2−Zn1−O1A	118.7(3)
O1−Zn1−O1A	83.4(5)	O2A-Zn1−O1A	129.4(3)
	Zn···Zn Distances		
Zn1···Zn2	3.098	Zn1···Zn3	3.095
	Zn−O−Zn Angles		
Zn1−O1−Zn3	99.7(4)	Zn2−O2−Zn1	99.9(3)

respectively, mediate Zn···Zn separations of 3.098 Å (Zn1···Zn2) and 3.095 Å (Zn1···Zn3).

The asymmetric unit of **2** contains one complete $[Cu_3(L1O)_4]^{2+}$ cation, two $[BF_4]^-$ anions, and two molecules of lattice MeCN. The $[Cu_3(L1O)_4]^{2+}$ cation contains three Cu^{2+} atoms in an almost linear array, and a slight "bending" of the trimer is observed as indicated by the Cu2−Cu1−Cu3 angle of 175.4°. The two terminal Cu^{2+} atoms are both coordinated by two tridentate $[L1O]^-$ ligands in a cis fashion with respect to the phenolate oxygen ligands, the Cu^{2+} ligand sphere thus being 6-coordinate N_4O_2. Each phenolate oxygen ligand further bridges to another Cu^{2+} atom, the central metal atom of the trimeric moiety, this being 4-coordinate O_4 ligated. The dihedral angle between the two $Cu_{terminal}O_2Cu_{central}$ planes is 46.8°, approximately midway between that for a square-planar and tetrahedral geometry (0 and 90°, respectively). This dihedral angle is a surprisingly large value for Cu^{2+}, where square-planar geometries are far more common than the quasi or flattened tetrahedral which are comparatively rare. This observation can be accounted for by steric interactions between the adjacent phenyl rings of the phenolate ligands which do not allow a square planar geometry but rather force the Cu1, O3, O4 plane to twist with respect to the Cu1, O1, O2 plane forming a flattened tetrahedral geometry. The O−Cu−O angles of the central Cu^{2+} atom of the trimer exhibit considerable deviation from regularity, with two angles O4−Cu1−O3 and O1−Cu1−O2 (82.3(3) and 82.9(3)°, respectively) highly compressed from either "ideal" square-planar or tetrahedral values (90 and 109.5°, respectively) due to formation of the $Cu_{terminal}O_2Cu_{central}$ chelate rings. The O4−Cu1−O1 and O3−Cu1−O2 angles (104.0(3) and 106.6(3)°, respectively) are much closer to "ideal" tetrahedral values. The terminal Cu^{2+} coordination geometries are distorted octahedral with the most highly distorted angles again being the $Cu_{terminal}O_2Cu_{central}$ chelate ring compressed O−Cu−O angles (average, 74.7°). For each terminal Cu^{2+} atom, two bonds are considerably elongated with respect to the other four (Cu3−O4, 2.109(7) Å; Cu3−N10, 2.151(9) Å; Cu2−O2, 2.200(7) Å; Cu2−N2, 2.239(10) Å) consistent with the Jahn−Teller effect. This indicates that the equatorial coordination plane is N_3O ligated (for Cu3, N12, N14, N16, O3; for Cu2; N4, N6, N8, O1), and the axial positions are taken by one N-donor and one O-donor (for Cu3, N10 and O4; for Cu2, N2 and O2). The Cu−O bond lengths of the central Cu^{2+} atom (average, 1.925 Å) are shorter than those of the shortest, equatorial Cu−O bonds of the terminal Cu^{2+} atoms (average, 2.031 Å); this is again attributable to the differences in the stereochemistries of these two types of metal atom. There is an asymmetry in the Cu−O−Cu bond angles of the $[Cu_3(L1O)_4]^{2+}$ cation, with two large (Cu1−O3−Cu3, 102.2(3)°, and Cu1−O1−Cu2, 104.4(3)°) and two small (Cu1−O4−Cu3, 100.0(3)°, and Cu1−O2−Cu2, 98.7(3)°). This asymmetry is due to the CuO_2Cu bridging mode for the linear trimer being "quasi" parallel-planar,[10−12] with the small Cu−O−Cu angle coming from an axially elongated terminal Cu−O bond and a relatively short flattened tetrahedral central Cu−O bond, and the large Cu−O−Cu angle resulting from a short equatorial terminal Cu−O bond and a short central Cu−O bond. These Cu−O−Cu bridging angles mediate Cu···Cu separations of 3.125 Å (Cu1···Cu2) and 3.091 Å (Cu1···Cu3).

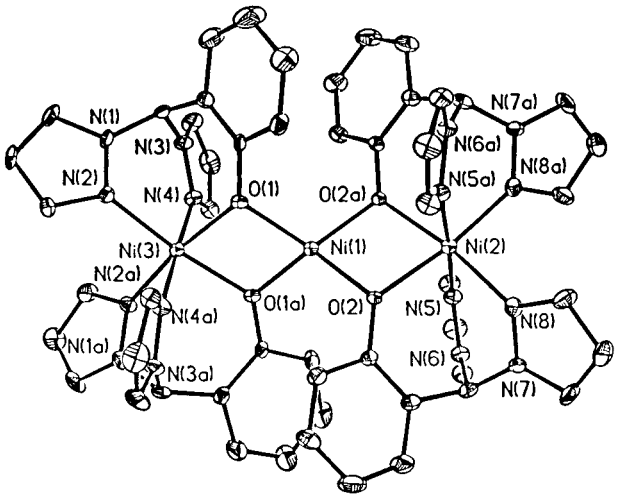

Figure 2. ORTEP diagram showing 30% probability ellipsoids and partial atomic labeling of **3**.

The linear trimeric cation of **3**, $[Ni_3(L1O)_4]^{2+}$ (Figure 2), contains three Ni^{2+} atoms located on a crystallographic C_2 axis with separations of 3.082 Å (Ni1···Ni2) and 3.055 Å (Ni1···Ni3). The two terminal Ni^{2+} atoms are each coordinated to two $[L1O]^-$ ligands in a tridentate manner, and the phenolate oxygen donor atoms are coordinated in a cis mode and each bridging

(10) Lintvedt, R. L.; Glick, M. D.; Tomlonovic, B. K.; Gavel, D. P.; Kuszaj, J. M. *Inorg. Chem.* **1976**, *15*, 1633.
(11) Calderazzo, F.; Marchetti, F.; Dell'Amico, G.; Pelizzi, G.; Colligiani, A. *J. Chem. Soc., Dalton Trans.* **1980**, 1419.
(12) Higgs, T. C.; Helliwell, M.; McInnes, E. J. L.; Mabbs, F. E.; Harding, C. J.; Garner, C. D. *J. Chem. Soc., Dalton Trans.* **1997**, 927.

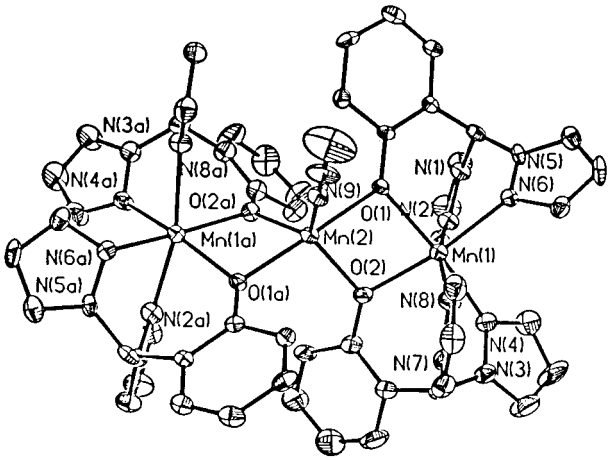

Figure 3. ORTEP diagram showing 30% probability ellipsoids and partial atomic labeling of **5**.

to a third Ni^{2+}, the central metal atom of the trimer. The O_4-ligated central Ni^{2+} has a flattened tetrahedral geometry with a dihedral angle of 60.4° between the two $Ni_{terminal}O_2Ni_{central}$ planes. The O−Ni−O angles of this metal atom show significant deviation from regularity, mainly due to induced compression of the O2−Ni−O2A and O1−Ni−O1A angles, to values of 80.3(3) and 81.4(4)°, by formation of the $Ni_{terminal}O_2Ni_{central}$ four-membered chelate ring which causes a corresponding expansion of the O1−Ni1−O2 and O1A-Ni1−O2A angles to values of 141.8(3) and 141.8(3)°. The terminal 6-coordinate Ni^{2+} atoms have distorted octahedral geometries, the main source of the geometric distortion again being due to compression of the O2−Ni2−OA (76.4(3)°) and O1−Ni3−O1A (76.8(3)°) angles by the formation of the $Ni_{terminal}O_2Ni_{central}$ chelate ring. The Ni−O bond distances of the central, flattened tetrahedral Ni^{2+} atom (average, 1.938 Å) are shorter than those of the distorted octahedral terminal Ni^{2+} atoms again due to the different stereochemistries of the central and terminal metal atoms. The phenolate oxygen bridging ligands make angles of 100.9(3)° (Ni1−O1−Ni3) and 101.4(2)° (Ni1−O2−Ni2) with the three Ni^{2+} atoms of the linear trimeric $[Ni_3(L1O)_4]^{2+}$ cation.

The coordination of the Co in **4** is nearly identical to that of its Ni analogue. The central CoO_4 adopts a flattened tetrahedral stereochemistry with a dihedral angle of 61.2° between the two $Co_{terminal}O_2Co_{central}$ planes and Co···Co separations of 3.088 Å (Co1···Co2) and 3.063 Å (Co1···Co3).

The crystal structure of **5** is considerably different from that of the other metal complexes. As in the Zn, Co, Ni, and Cu analogues the $[Mn_3(L1O)_4(MeCN)]^{2+}$ cation contains one Mn^{2+} atom (Mn1, Figure 3) coordinated to two tridentate $[L1O]^-$ ligands with the two phenolate oxygens orientated cis to each other; these also bridge to a second Mn^{2+} atom (Mn2) located on a crystallographic C_2 axis (which generates the other half of the cation). However, in this case Mn2 is further coordinated to an exogenous ligand, a MeCN solvent molecule which is also sitting on the C_2 axis. The two symmetry-related terminal Mn^{2+} atoms are therefore N_4O_2 ligated, 6-coordinate, in a distorted octahedral geometry while the central Mn^{2+} atom is N_1O_4 ligated, giving a 5-coordinate slightly distorted trigonal bipyramidal coordination geometry. The structural index, τ (where $\tau = (\beta - \alpha)/60$, where β and α are the two largest coordination angles; $\tau = 0$ for square-based pyramidal geometry, and $\tau = 1$ for trigonal bipyramidal geometry),[13] has a value of 0.87. The equatorial plane of the TBP is defined by two bridging phenolate oxygen donors (O2 and O2A) and the nitrogen of the coordinated MeCN solvent molecule. The axial positions contain the two bridging phenolate oxygen ligands (O1 and O1A) with a trans O1−Mn2−O1A angle of 174.3-(3)°, close to the ideal value of 180°. The equatorial Mn2−O bonds of Mn2 are somewhat shorter at 2.005(6) Å than the axial Mn2−O bonds (2.139(6) Å). The O2A−Mn2−O2 angle (115.4(4)°) of the equatorial plane is compressed from the ideal trigonal value of 120°, and the two N−Mn2−O angles of this plane (122.3(2)°) are slightly expanded. The observed slight distortions in the equatorial plane angles of this stereochemistry are a result of accommodating the formation of the four-membered $Mn_{terminal}O_2Mn_{central}$ chelate ring in forming the linear trimeric moiety. The Mn−O−Mn bridging angles are asymmetric with Mn1−O1−Mn2 having a value of 97.2(2)° and Mn1−O2−Mn2 a value of 101.0(3)°. The phenolate oxygen bridging atoms mediate a Mn1···Mn2 separation of 3.215 Å, significantly longer than the other members of this series (vide supra). The nonlinear Mn1−Mn2−Mn1A angle of 161.8° indicates that this system is perhaps better described as a isosceles triangular trimer with two short di-μ-oxygen-bridged Mn···Mn distances and one nonbridged long Mn···Mn separation. This Mn1−Mn2−Mn1A bend is a result of the equatorial/axial nature of the phenolate oxygen bridges caused by the addition of the fifth ligand to the central metal atom.

Electronic Properties. The band positions and intensities in the electronic spectra of $[Cu_3(L1O)_4][BF_4]_2\cdot 3H_2O$, $[Ni_3(L1O)_4][ClO_4]_2\cdot H_2O$ and $[Co_3(L1O)_4][BF_4]_2\cdot 2H_2O$ in MeCN solution are summarized in Table 7. For $[Ni_3(L1O)_4][ClO_4]_2\cdot H_2O$ and $[Co_3(L1O)_4][BF_4]_2\cdot 2H_2O$ band assignments were made on the basis of the intensities of the observed absorptions since the intensities of the d−d bands in a T_d or pseudotetrahedral crystal field are more intense by about a factor of 10 than those in an octahedral field due to the absence of a center of symmetry.[14] Therefore the transitions due to the flattened tetrahedral central metal atom of these two systems largely dominate the visible region of their respective electronic spectra. However for $[Ni_3(L1O)_4][ClO_4]_2\cdot H_2O$ the lowest energy transition in its spectrum (near 820 nm) has an energy and intensity ($\epsilon = 12$ per terminal Ni^{2+}) consistent with either an $^3A_{2g} \rightarrow {}^3T_{2g}$ or $^3A_{2g} \rightarrow {}^3T_{1g}$ octahedral crystal field transition.

In $[Cu_3(L1O)_4][BF_4]_2\cdot 3H_2O$ the visible region of the spectrum is dominated by an intense asymmetric absorption centered approximately 480 nm which is made up from two overlapping bands (452 nm, $\epsilon = 3856$, and 512 sh, $\epsilon = 3044$). The intensity of this absorption clearly precludes it being a d−d transition; hence, this feature is assigned as being due to phenolate oxygen to Cu^{II} charge-transfer transitions. It is tempting to infer that one of these PhO−Cu^{II} CT bands is due terminal Cu^{2+} CT and the other to central Cu^{2+} CT in the $[Cu_3(L1O)_4]^{2+}$ cation; however, more detailed studies are needed to verify this point. The other transition in the visible region of the electronic spectrum of this complex is a much less intense band at 762 nm ($\epsilon = 253$), which is the expected d−d transition.

Magnetism and EPR. We have obtained variable-temperature magnetic data on compounds **2**−**5** and completed a preliminary analysis (Figure 4). A more detailed analysis of the data is beyond the scope of this work and will be reported in a separate publication along with comparative data on the dinuclear and triangular trinuclear complexes we have previously

(13) (a) Addison, A. W.; Rao, T. N.; Reedijk, J.; van Rijn, J.; Verschoor, G. C. *J. Chem. Soc., Dalton Trans.* **1984**, 1349. (b) Zoeteman, M.; Bouwman, E.; de Graff, R. A. G.; Driessen, W. L.; Reedijk, J.; Zanello, P. *Inorg. Chem.* **1990**, *29*, 3487.

(14) Nicholls, D. *Comprehensive Inorganic Chemistry*; Bailar, J. C., Emeleus, H. J., Nyholm, R., Trotman-Dickenson, A. F., Eds.; Pergamon Press: Oxford, U.K., 1973; Vol. 3, pp 1152−1159.

Table 3. Bond Distances (Å) and Angles (deg) for $[Cu_3(L1O)_4][BF_4]_2 \cdot 2MeCN$

Cu3 Bond Distances			
Cu3−O3	2.038(6)	Cu3−O4	2.109(7)
Cu3−N10	2.151(9)	Cu3−N12	2.045(8)
Cu3−N14	2.066(9)	Cu3−N16	2.061(9)
Cu3 Angles			
O3−Cu3−N10	92.3(3)	O4−Cu3−N10	166.7(3)
O3−Cu3−N12	84.5(3)	O4−Cu3−N12	95.4(3)
N10−Cu3−N12	88.7(3)	O3−Cu3−N14	169.5(3)
O4−Cu3−N14	95.6(3)	N10−Cu3−N14	97.0(4)
N12−Cu3−N14	90.8(4)	O3−Cu3−N16	97.3(3)
O4−Cu3−N16	83.7(3)	N10−Cu3−N16	92.7(3)
N12−Cu3−N16	177.7(4)	N14−Cu3−N16	87.1(3)
O3−Cu3−O4	75.5(3)		
Cu2 Bond Distances			
Cu2−O1	2.024(7)	Cu2−O2	2.200(7)
Cu2−N2	2.239(10)	Cu2−N4	1.997(7)
Cu2−N6	2.047(10)	Cu2−N8	1.994(7)
Cu2 Angles			
O1−Cu2−O2	73.9(3)	O1−Cu2−N2	93.4(4)
O2−Cu2−N2	166.3(3)	O1−Cu2−N4	85.5(3)
O2−Cu2−N4	96.4(3)	N2−Cu2−N4	87.7(3)
O1−Cu2−N6	168.8(3)	O2−Cu2−N6	95.0(3)
N2−Cu2−N6	97.8(4)	N4−Cu2−N6	93.8(4)
O1−Cu2−N8	92.4(3)	O2−Cu2−N8	82.5(3)
N2−Cu2−N8	93.0(3)	N4−Cu2−N8	177.8(4)
N6−Cu2−N8	88.2(3)		
Cu1 Bond Distances			
Cu1−O1	1.931(6)	Cu1−O2	1.911(7)
Cu1−O3	1.933(6)	Cu1−O4	1.924(7)
Cu1 Angles			
O1−Cu1−O2	82.9(3)	O1−Cu1−O3	146.7(2)
O2−Cu1−O3	106.6(3)	O1−Cu1−O4	104.0(3)
O2−Cu1−O4	152.4(2)	O3−Cu1−O4	82.3(3)
Cu···Cu Distances			
Cu1···Cu2	3.125	Cu1···Cu3	3.091
Cu2−Cu1−Cu3 Angle			
Cu2−Cu1−Cu	3175.4		
Cu−O−Cu Angles			
Cu1−O3−Cu3	102.2(3)	Cu1−O4−Cu3	100.0(3)
Cu1−O2−Cu2	98.7(3)	Cu1−O1−Cu2	104.4(3)

Table 4. Bond Distances (Å) and Angles (deg) for $[Ni_3(L1O)_4][ClO_4]_2 \cdot MeCN \cdot 0.5H_2O$

Ni2 Bond Distances			
Ni3−O1	2.029(6)	Ni3−N2	2.065(8)
Ni3−N4	2.052(7)	Ni3−O1A	2.029(6)
Ni3−N2A	2.065(8)	Ni3−N4A	2.052(7)
Ni2 Angles			
O2−Ni2−N5	85.1(3)	O2−Ni2−N8	94.7(3)
N5−Ni2−N8	87.4(3)	O2−Ni2−O2A	76.4(3)
N5−Ni2−O2A	92.5(3)	N8−Ni2−O2A	171.0(3)
O2−Ni2−N5A	92.5(3)	N5−Ni2−N5A	177.1(4)
N8−Ni2−N5A	94.6(3)	O2A-Ni2−N5A	85.1(3)
O2−Ni2−N8A	171.0(3)	N5−Ni2−N8A	94.6(3)
N8−Ni2−N8A	94.3(4)	O2A-Ni2−N8A	94.7(3)
N5A-Ni2−N8A	87.4(3)		
Ni3 Bond Distances			
Ni3−O1	2.029(6)	Ni3−N2	2.065(8)
Ni3−N4	2.052(7)	Ni3−O1A	2.029(6)
Ni3−N2A	2.065(8)	Ni3−N4A	2.052(7)
Ni3 Angles			
O1−Ni3−N4	86.5(3)	N2−Ni3−N4	88.3(3)
O1−Ni3−O1A	76.8(3)	N2−Ni3−O1A	170.8(3)
N4−Ni3−O1A	92.6(3)	O1−Ni3−N2A	170.8(3)
N2−Ni3−N2A	95.0(4)	N4−Ni3−N2A	92.5(3)
O1A-Ni3−N2A	94.1(3)	O1−Ni3−N4A	92.6(3)
N2−Ni3−N4A	92.5(3)	N4−Ni3−N4A	178.8(4)
O1A-Ni3−N4A	86.5(3)	N2A-Ni3−N4A	88.3(3)
O1−Ni3−N2	94.1(3)		
Ni1 Bond Distances			
Ni1−O1	1.932(6)	Ni1−O2	1.944(5)
Ni1−O2A	1.944(5)	Ni1−O1A	1.932(6)
Ni1 Angles			
O1−Ni1−O2	141.8(3)	O1−Ni1−O1A	81.4(4)
O2−Ni1−O1A	111.6(2)	O1−Ni1−O2A	111.6(2)
O2−Ni1−O2A	80.8(3)	O1A-Ni1−O2A	141.8(3)
Ni···Ni Distances			
Ni1···Ni2	3.082	Ni1···Ni3	3.055
Ni−O−Ni Angles			
Ni1−O1−Ni3	100.9(3)	Ni1−O2−Ni2	101.4(2)

reported.[1,2] In general the data have been fit to the HDVV (Heisenberg−Dirac−Van Vleck) spin Hamiltonian for linear trinuclear complexes (eq 1), where $S_1 = S_2 = S_3$ and $J_{12} = J_{23}$.

$$\underset{S_1}{A}\text{---}\underset{S_2}{A}\text{---}\underset{S_3}{A}$$

$$H_{exch} = -2[J_{12} \cdot S_1 \cdot S_2 + J_{23} \cdot S_2 \cdot S_3 + J_{13} \cdot S_1 \cdot S_3] \qquad (1)$$

The theoretical expression for $\chi_m T$ can be found in ref 7. While this approach generally yielded satisfactory results, in some cases a more detailed crystal field treatment may be warranted.

χT per mole of complex for **4** has an essentially temperature-independent value of ca. 10.6 $cm^3\ mol^{-1}$ K over the range from 300 to 50 K. Below 50 K it rises sharply to a value of 12.1 $cm^3\ mol^{-1}$ K which is close to that (12.37) expected for an $S = {}^9/_2$ ground state resulting from ferromagnetic coupling of three hs d^7 Co^{2+} ions before falling again at very low temperature. This behavior is consistent with a very strongly ferromagnetically coupled system with significant zero-field splitting (ZFS). The lack of a temperature dependence to χT over most of the range makes it impossible to determine a J value, but it must be greater than 60 cm^{-1}. The EPR spectrum of **4** at 10 K (Figure 5) shows a rhombic signal with g values near 10, 2.7, and 1.6 and hyperfine splitting from the $I = {}^7/_2$ Co observable in the low-field feature, consistent with an $S = {}^9/_2$ ground state.

For **2**, χT varies from about 4.3 at 300 K to 0.45 $cm^3\ mol^{-1}$ K at 2 K. The value expected for an $S = {}^1/_2$ ground state would be 0.375 suggesting significant antiferromagnetic coupling of the three Cu^{2+} ions. Fits of the data give an adjacent coupling of $-19.95\ cm^{-1}$, a terminal coupling of 0 cm^{-1}, g-octahedral 2.140, g-tetrahedral 2.103, and TIP of 1.10×10^{-2}.[15] The 20 K EPR spectrum shows an axial signal centered near $g = 2$, typical of a tetragonally distorted copper environment and consistent with an $S = {}^1/_2$ ground state.

The value of χT for the Mn complex, **5**, drops from about 20 $cm^3\ mol^{-1}$ K at room temperature to 4.5 at 2 K. The low-temperature limit is nearly exactly that expected for an $S = {}^5/_2$ ground state arising from an antiferromagnetically coupled system as is the hyperfine split EPR spectrum at 20 or 4.2 K.[16] The magnetic data were again fit to a spin Hamiltonian which

(15) Although in theory there are two independent coupling constants, one for the adjacent and one for the terminal interactions, there is no *mathematical* justification for including this second J value as (a) the fits were imperceptibly improved by the additional parameter and (b) if two J values were used they were highly correlated and averaged to a value the same as that of the single J reported; hence, as is commonly done, the terminal coupling, J_{13}, was set to zero. Kessissoglou, D. P.; Kirk, M. L.; Lah, M. S.; Li, X.; Raptopoulou, C.; Hatfield, W. E.; Pecoraro, V. L. *Inorg. Chem.* **1992**, *31*, 5424.

Table 5. Bond Distances (Å) and Angles (deg) for $[Co_3(L1O)_4][BF_4]_2$·MeCN

Co2 Bond Distances			
Co2−O2	2.069(4)	Co2−N5	2.093(5)
Co2−N8	2.117(5)	Co2−O2A	2.069(4)
Co2−N5A	2.093(5)	Co2−N8A	2.117(5)
Co2 Angles			
O2−Co2−N5	84.8(2)	O2−Co2−N8	93.8(2)
N5−Co2−N8	86.0(2)	O2−Co2−O2A	77.5(2)
N5−Co2−O2A	93.8(2)	N8−Co2−O2A	171.2(2)
O2−Co2−N5A	93.8(2)	N5−Co2−N5A	178.2(3)
N8−Co2−N5A	95.2(2)	O2A-Co2−N5A	84.8(2)
O2−Co2−N8A	171.2(2)	N5−Co2−N8A	95.2(2)
N8−Co2−N8A	95.0(3)	O2A-Co2−N8A	93.8(2)
N5A−Co2−N8A	86.0(2)		
Co3 Bond Distances			
Co3−O1	2.067(4)	Co3−N2	2.088(5)
Co3−N4	2.083(5)	Co3−O1A	2.067(4)
Co3−N2A	2.088(5)	Co3−N4A	2.083(5)
Co3 Angles			
O1−Co3−N2	86.0(2)	O1−Co3−N4	92.8(2)
N2−Co3−N4	87.8(2)	O1−Co3−O1A	78.1(2)
N2−Co3−O1A	93.1(2)	N4−Co3−O1A	170.8(2)
O1−Co3−N2A	93.1(2)	N2−Co3−N2A	178.8(3)
N4−Co3−N2A	93.0(2)	O1A-Co3−N2A	86.0(2)
O1−Co3−N4A	170.8(2)	N2−Co3−N4A	93.0(2)
N4−Co3−N4A	96.3(3)	O1A-Co3−N4A	92.8(2)
N2A-Co3−N4A	87.8(2)		
Co1 Bond Distances			
Co1−O1	1.955(4)	Co1−O2A	1.962(4)
Co1−O2	1.962(4)	Co1−O1A	1.955(4)
Co1 Angles			
O1−Co1−O2	140.5(2)	O1−Co1−O1A	83.6(2)
O2−Co1−O1A	110.4(1)	O1−Co1−O2A	110.4(1)
O2−Co1−O2A	82.6(2)	O1A-Co1−O2A	140.5(2)
Co···Co Distances			
Co1···Co2	3.088	Co1···Co3	3.063
Co−O−Co Angles			
Co1−O2−Co2	99.9(2)	Co1−O1−Co3	99.1(2)

gave values of J_{12} of -1.8 cm^{-1}, J_{13} of 0, *g*-octahedral 1.87, *g*-tetrahedral 1.68, and TIP of 3.2×10^{-2}. Thus although the coupling is still overall antiferromagnetic, it is considerably weaker for Mn as compared to Cu. Interestingly the *J* value for trinuclear **5** which has phenolate oxygen bridges between Mn^{2+} centers of differing geometry is virtually the same as that seen in an analogous actetate-bridged, all octahedral, Mn trimer despite the somewhat shorter Mn−Mn distances in the former.[16]

Finally, for the Ni^{2+} trimer, **3**, χT decreases from about 6 at 300 K to 1.95 cm^3 mol^{-1} K at 2 K suggesting an $S = 1$ ground state with some significant population of higher moment states of a spin ladder. In this case adequate fits of the data required *both* terminal and adjacent coupling constants with J_{12} of $+22.7$ cm^{-1}, J_{13} -23.18 cm^{-1}, *g*-octahedral 2.201, *g*-tetrahedral 1.918, and TIP of 8.9×10^{-3}. Attempts to fit the data for **3** with only a single *J* gave approximately 1000-fold greater χ^2 values ($\chi^2 = \sum(\text{expt} - \text{calcd/expt})^2$). The $S = 1$ ground-state assignment is also consistent with the lack of an observable low-temperature EPR spectra as expected for an integral spin system.

Discussion

The tridentate "heteroscorpionate" ligand (2-hydroxyphenyl)-bis(pyrazolyl)methane forms stable linear homometallic trimeric cations of the form $[(L1O)_2MMM(L1O)_2]^{2+}$ with the M^{2+} ions Zn^{2+}, Cu^{2+}, Ni^{2+}, Co^{2+}, and Mn^{2+}. These trimeric cations exhibit a remarkable consistency in their overall gross structure throughout the series, with the sole exception of Mn^{2+} which possesses a 5-coordinate, rather than 4-coordinate, central metal atom. For the Zn^{2+}, Cu^{2+}, Ni^{2+}, and Co^{2+} cations in fact, apart from the obvious metal-dependent (small) variations in M−L bond distances and angles, the only major structural difference between these species is the dihedral angle, ω, of the (flattened) tetrahedral central metal atom (46.8° (Cu), 60.4° (Ni), and 61.2° (Co)). This sort of consistency in molecular structure, for a particular ligand type, across the first row of the transition metals is rarely observed, the other striking example being that described by Wieghardt et al., with the hexadentate ligand 1,4,7-tris(3,5-dimethyl-2-hydroxybenzyl)-1,4,7-triazacyclononane and its thio analogue.[4−6] These ligands also form phenolate

Table 6. Bond Distances (Å) and Angles (deg) for $[Mn_3(L1O)_4(MeCN)][ClO_4]_2$ ·1.4MeCN

Mn1 Bond Distances			
Mn1−O2	2.111(6)	Mn1−O1	2.149(6)
Mn1−N4	2.227(9)	Mn1−N2	2.183(9)
Mn1−N8	2.257(9)	Mn1−N6	2.211(8)
Mn1 Angles			
O1−Mn1−O2	77.8(2)	O2−Mn1−N2	108.8(3)
O1−Mn1−N2	84.4(3)	O1−Mn1−N4	165.1(3)
O2−Mn1−N4	95.8(3)	N2−Mn1−N4	85.1(3)
O2−Mn1−N6	162.9(3)	O1−Mn1−N6	92.0(3)
N4−Mn1−N6	97.3(3)	N2−Mn1−N6	83.3(3)
O1−Mn1−N8	110.2(3)	O2−Mn1−N8	79.0(3)
N2−Mn1−N8	165.0(3)	N4−Mn1−N8	81.3(3)
N6−Mn1−N8	92.1(3)		
Mn2 Bond Distances			
Mn2−O2	2.055(6)	Mn2−O1	2.139(6)
Mn2−O1A	2.139(6)	Mn2−O2A	2.055(6)
Mn2−N9	2.272(17)		
Mn2 Angles			
O2−Mn2−N9	122.3(2)	O1−Mn2−O2	79.2(2)
O1−Mn2−O1A	174.3(3)	O1−Mn2−N9	87.2(2)
N9−Mn2−O1A	87.2(2)	O2−Mn2−O1A	103.9(2)
O2−Mn2−O2A	115.4(4)	O1−Mn2−O2A	103.9(2)
N9−Mn2−O2A	122.3(2)	O1A-Mn2−O2A	79.2(2)
Mn1···Mn2 Distance			
Mn1···Mn2	3.215		
Mn1−Mn2−Mn1A Angle			
Mn1−Mn2−Mn1A	161.8		
Mn−O−Mn Angles			
Mn1−O1−Mn2	97.2(2)	Mn1−O2−Mn2	101.0(3)

Table 7. Summary of Electronic Spectra for $[Cu_3(L1O)_4][BF_4]_2$, $[Ni_3(L1O)_4][ClO_4]_2$·H_2O, and $[Co_3(L1O)_4][BF_4]_2$·$2H_2O$ in MeCN Solution

complex	electronic band posns, nm (cm^{-1})	extinction coeff ϵ, M^{-1} cm^{-1}	proposed band assgnt
$[Cu_3(L1O)_4][BF_4]_2$	328 sh (30 490)	4300	L → Cu^{II} CT
	452 (22 030)	3856	PhO−Cu^{II} CT
	512 sh (19 530)	3044	PhO−Cu^{II} CT
	762 (13 120)	253	d−d
$[Ni_3(L1O)_4][ClO_4]_2$·H_2O	354 sh (28 250)	1510	L → Ni^{II} CT
	454 sh (22 025)	120	d−d (tet)
	492 (20 325)	106	d−d (tet)
	628 (15 925)	48	d−d (tet)
	ca. 820 (12 195)	23	d−d (oct)
$[Co_3(L1O)_4][BF_4]_2$·$2H_2O$	346 sh (28 900)	934	L → Co^{II} CT
	472 (21 185)	140	d−d (tet)
	564 sh (17 730)	152	d−d (tet)
	584 (17 125)	171	d−d (tet)

(16) Tangoulis, V.; Malamatari, D. A.; Soulti, K.; Stergiou, V.; Raptopoulou, C. P.; Terzis, A.; Kabanous, T. A.; Kessissooglou, D. P. *Inorg. Chem.* **1996**, *35*, 4974.

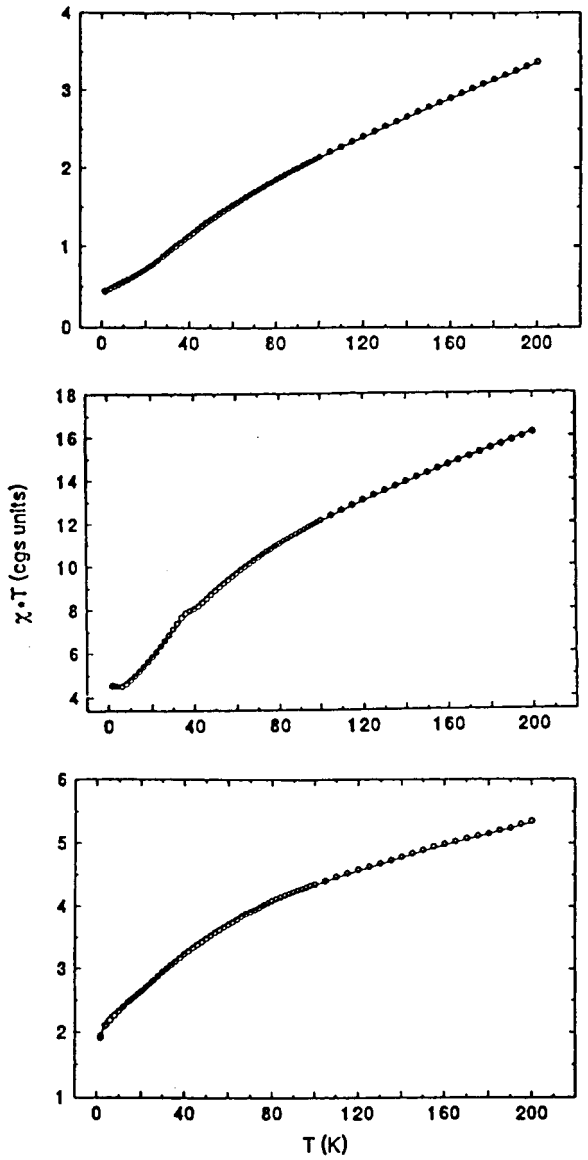

Figure 4. Plots of χT vs T along with fits of the data to the HDVV Hamiltonian as described in the text for the Cu, **2** (top), Mn, **5** (middle), and Ni, **3** (bottom), trinuclear complexes.

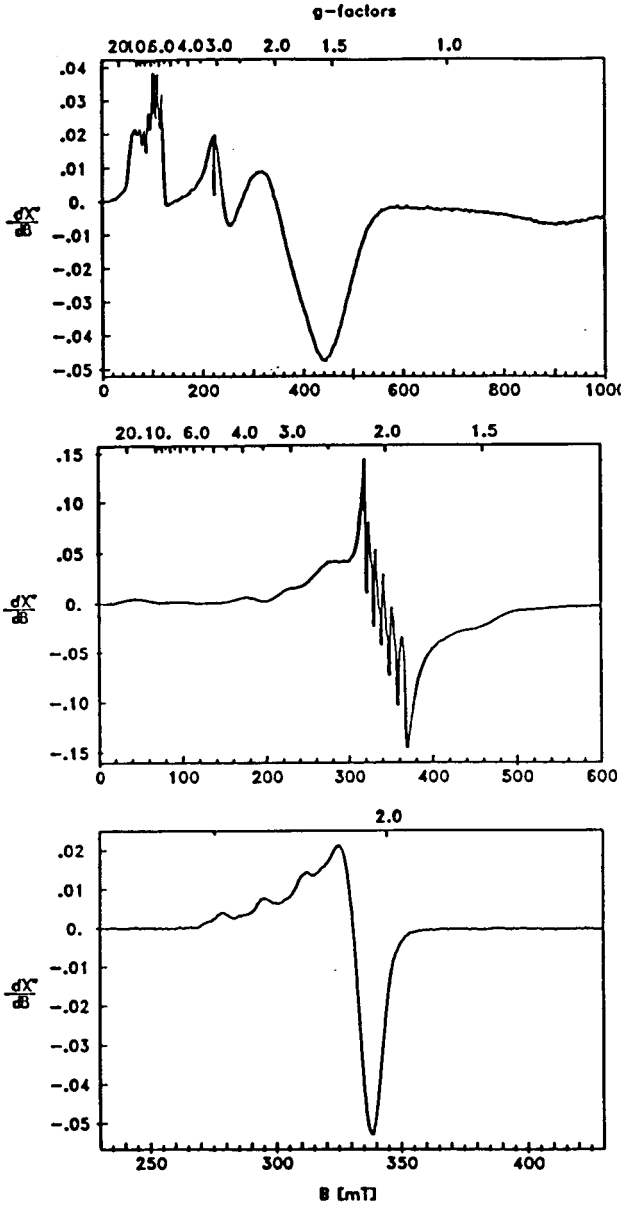

Figure 5. EPR spectra of solid samples of the Co, **4** (top), Mn, **5** (center), and Cu, **2** (bottom), trinuclear complexes at 20 K. Conditions: 20 μW/40 dB, 9.642 GHz, 1 G modulation amplitude.

(thiolate)-bridged linear trinuclear complexes of the form $[LMMML]^{n+}$, but the trimeric unit is composed of three face-sharing octahedra, in contrast to the octahedral/tetrahedral/octahedral motif found in **2**−**5**. While other examples of linear trimeric homometallic complexes with O- or S-bridges are very common, their specific structural properties seem to be mediated mainly by the structural preferences of the metal (*e*.g. stereochemical, coordination number, etc.) rather than by the ligand, which leads to gross structural differences in a series of metal complexes. For example, linear trimeric Ni^{2+} complexes often possess trinuclear units in a "chair" conformation with square-planar or octahedral, terminal, and central Ni^{2+} atoms.[17−20] For Cu^{2+} trinuclear species (commonly synthesized from Schiff-base ligands) "flat",[21,22] "bent", and "chair"[23] conformations exist with the terminal and central Cu^{2+} atoms in 4-, 5-, or 6-coordinate coordination environments. One exception is the complex $[Cu^{II}_3(OCH_2CH_2CH_2NH_2)_4(dmf)][Cu^{I}_6I_{10}]$,[24] which possesses a square-planar/flattened tetrahedral/square-planar motif with a dihedral angle, ω, about the central Cu^{2+} of 40°, thus possessing some similarity to the central Cu^{2+} of the $[Cu_3(L1O)_4]^{2+}$ cation. Co^{2+} trinuclear species also often possess either "chair"[24] or "bent"[25] conformations with octahedral terminal and central Co^{2+} atom geometry.

Several characteristics of the L1OH ligand mediate important structural features in the $[M_3(L1O)_4]^{2+}$ cations formed from it, providing a major contribution to the overall consistency of structure throughout the first-row transition metal series. For

(17) Turner, M. A.; Driessen, W. L.; Reedijk, J. *Inorg. Chem.* **1990**, *29*, 3331.
(18) Bullen, G. J.; Mason, R.; Pauling, P. *Inorg. Chem.* **1965**, *4*, 456.
(19) Wei, C. H.; Dahl, L. F. *Inorg. Chem.* **1970**, *9*, 1878.
(20) Barrera, H.; Suades, J.; Perucaud, M. C.; Brianso, J. L. *Polyhedron*. **1984**, *3*, 839.
(21) Chiari, B.; Piovesana, O.; Tarantelli, T.; Zanazzi, P. F. *Inorg. Chem.* **1985**, *24*, 4615.
(22) Ferguson, G.; Langrick, R.; Parker, D.; Matthes, K. E. *J. Chem. Soc., Chem. Commun.* **1985**, 1609.
(23) Epstein, J. M.; Figgis, B. N.; White, A. H.; Willis, A. C. *J. Chem. Soc., Dalton Trans.* **1974**, 1954.
(24) Myllyviita, S.; Sillanpaa, R. *J. Chem. Soc., Dalton Trans.* **1994**, 2125.
(25) Fukuhara, C.; Asato, E.; Shimoji, T.; Katsura, K.; Mori, M.; Matsumoto, K.; Ooi, S. *J. Chem. Soc., Dalton Trans.* **1987**, 1305.

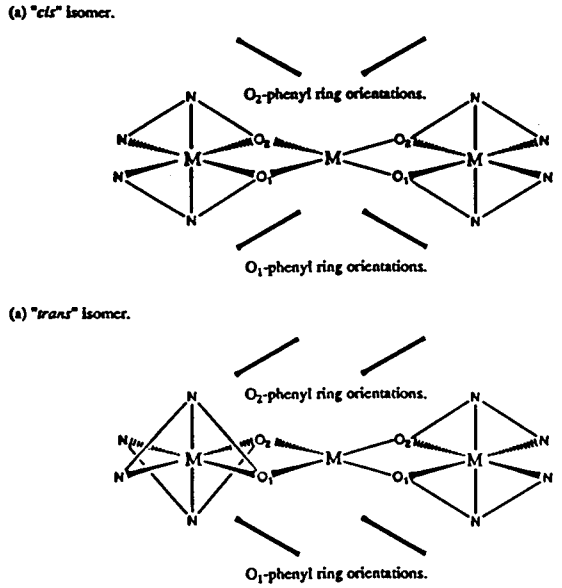

Figure 6. Schematic diagram showing the "cis" and "trans" isomers present in the linear trinuclear complexes.

example the intramolecular steric interactions between the bridging phenolate rings of terminal metal atoms precludes the formation of a square-planar geometry about the central metal and encourages formation of tetrahedral type geometries even when these are not preferred. Most notable in this regard is the $[Cu_3(L1O)_4]^{2+}$ cation with a dihedral angle of 46.8°, considerably larger those commonly observed in 4-coordinate Cu^{II} centers where dihedral angles larger than 15° are rare. The induced tetrahedral geometry of the central metal also prevents the adoption of the more common "chair" conformation in the trinuclear unit observed in many other Ni^{2+} and Co^{2+} systems.[17−20,25] The the flattened tetrahedral geometry adopted by both the Ni^{2+} and Co^{2+} with dihedral angles, ω, of 60.4 and 61.2°, respectively, is somewhat unexpected considering that regular tetrahedral geometries are quite common for both of these metals and that the steric interactions between the phenyl rings would seem to encourage such a geometry. While for Ni^{2+} square-planar geometries are also commonly observed and so stereochemical flexibility between these two extremes is not unreasonable, such is not the case for Co^{2+}.

Another significant structural feature only becomes evident upon close examination of the $[Cu_3(L1O)_4]^{2+}$, $[Ni_3(L1O)_4]^{2+}$, and $[Co_3(L1O)_4]^{2+}$ cations and reveals an apparent stacking interaction between the phenyl rings of the bridging phenolates. The fact that the stacked phenyl rings are not exactly parallel with dihedral angles, ϕ, of 21−22° and that the average separation of the rings is approximately 3.8−3.9 Å suggests that these are not true π-stacking interactions in the usual sense.[27] Interestingly the $[Zn_3L1O)_4]^{2+}$ cation does not show this stacking and indeed the phenyl rings are almost orthogonal to each other. We first attributed this to the difference in ω values between the Cu^{2+}, Ni^{2+}, Co^{2+}, and Zn^{2+} complexes; however, it became obvious that such cannot account for this large difference in phenyl ring disposition. This brought to our attention a subtle form of "cis" and "trans" isomerism present in these $[M_3(L1O)_4]^{2+}$ cations and which is illustrated schematically in Figure 6. The "cis" isomer has the two M-*OPh*−M−*OPh*−M bridging phenolate-O $[L1O]^-$ ligands (the two O1 or O2 $[L1O]^-$ ligands within the MO_2MO_2M moiety in Figure 6) chelated so that the "axial" pyrazoles of these two $[L1O]^-$ ligands are *both* located below or above the $N_2MO_2MO_2MN_2$ plane, and the other two $[L1O]^-$ ligands of the trinuclear unit have their pyrazoles located on the opposite side of this plane. The Zn complex, **1**, adopts this structure. For the "trans" isomer, the M−*OPh*−M−*OPh*−M bridging phenolate-O $[L1O]^-$ ligands (the two O1 or O2 $[L1O]^-$ ligands within the MO_2MO_2M moiety in Figure 6) are chelated so that one of the "axially" coordinated pyrazoles, of this $[L1O]^-$ ligand pair, is positioned above the $N_2MO_2MO_2MN_2$ plane and the other below this plane. This isomer is observed in the Co^{2+}, Ni^{2+}, and Cu^{2+} cations.

The Mn^{2+} complex is somewhat anomalous in this series of compounds in that the central Mn^{2+} atom is *five coordinate* with a trigonal bipyramidal geometry. High-spin d^5 Mn^{2+} has no CFSE and hence no preference for any particular stereochemistry with coordination numbers of 4, 5, and 6 all relatively common. Although 6-coordination about the central Mn^{2+} atom is precluded by the steric hindrance imposed by the four phenolate rings, the degree of steric hindrance imposed by these ligands is apparently insufficient to prevent 5-coordination, provided that only a small exogenous ligand occupies the fifth coordination site. Examination of Figure 4 clearly indicates that steric interactions within the Mn^{2+} trinuclear unit do not appear to be appreciably different than those in the Zn^{2+}, Cu^{2+}, Ni^{2+}, and Co^{2+} trinuclear complexes, and as a result, it is not immediately clear why the Cu^{2+} and Ni^{2+} complexes (metals for which 5-coordination is possible) do not similarly accommodate an exogenous MeCN ligand, since crystallization conditions were the same for all these compounds.

Variable-temperature magnetic and EPR data have been used to identify the low-temperature ground magnetic states and indicate that the overall couplings in the $[Cu_3(L1O)_4]^{2+}$ and $[Ni_3(L1O)_4]^{2+}$ cations are modestly *antiferromagnetic*, in the $[Co_3(L1O)_4]^{2+}$ cation *strongly ferromagnetic*, and in the $[Mn_3(L1O)_4(MeCN)]^{2+}$ cation weakly *antiferromagnetic*. The Ni complex, **3**, can be compared to the Ni dimers and trinuclear complexes prepared by Wieghardt and Ginsberg.[4−6] In the case of the face-sharing octahedral/octahedral/octahedral systems with acac or phenolate bridges the overall ground state is $S = 3$ with a dominant ferromagnetic adjacent coupling (ca. $+12-15$ cm^{-1}) and a smaller antiferromagnetic (-4 to -6 cm^{-1}) terminal interaction.[6] The ferromagnetic ground state is attributed to the orthogonality of the magnetic orbitals due to the near 90° bridging angle. In the case of the thiolate-bridged analogue, the relative sign of the coupling has been reversed with $J_{12} = -28$ cm^{-1} and $J_{13} = +12$ cm^{-1}, the resulting ground state being $S = 1$.[6] The rationalization here is that the more acute bridging angle (ca. 75°) removes the accidental orthogonality between the magnetic orbitals and that a new antiferromagnetic superexchange pathway becomes available due to the better energy match between the metal 3d orbital and the sulfur 3s orbitals. For the phenolate-bridged dinuclear octahedral/tetrahedral nickel complex the adjacent interaction is also antiferromagnetic but of larger magnitude (perhaps due to the lack of the competing ferromagnetic terminal interaction).[5] The angles in this system are also very acute leading to a loss of orthogonality between the magnetic orbitals (with its attendant ferromagnetic interaction) and an antiferromagnetic superexchange pathway, involving net overlap of the type $e_g||p||t_2$, becomes available, resulting in the $S = 1$ ground state.[5] In the case of **3** we see adjacent and terminal couplings that are nearly equal in magnitude but

(26) Solari, E.; Floriani, C.; Cunningham, D.; Higgins, T.; McArdle, P. *J. Chem. Soc., Dalton Trans.* **1991**, 3139.
(27) Hunter, C. A.; Sanders, J. K. M. *J. Am. Chem. Soc.* **1990**, *112*, 5525.

opposite in sign which also lead to an $S = 1$ ground state. However here the bridging angles are greater than 90° (average ca. 100°).

The weak to modest overall antiferromagnetism (the terminal coupling appears to be near zero) in the Cu and Mn complexes is not really surprising and can probably be rationalized via a number of different models (such as the so-called "crossed interactions"[28]). However, there seems to be no simple model that can explain the magnetic results for **all** four complexes. In particular the very strong ferromagnetic interactions between the Co^{2+} ions in **4** appears to be unprecedented. These initial results are clearly indicative of spin−spin interactions displaying considerable variety in behavior between the different metals. Thus the synthesis and characterization of the magnetic properties of *octahedral/tetrahedral* dimers of the type $[M(L1O)_2MCl_2]$ and heterometallic species where the nature of the metal in the terminal and central positions can be varied are required to more fully elucidate the spin−spin interactions. These studies are currently in progress and will be detailed in a future paper.

Acknowledgment. This work was supported by Grant AI-1157 from the Robert A. Welch Foundation. The NSF-ILI Program Grant USE-9151286 is acknowledged for partial support of the X-ray diffraction facilities at Southwest Texas State University.

Supporting Information Available: Complete listings of atomic positions, bond lengths and angles, anisotropic thermal parameters, hydrogen atom coordinates, and data collection and crystal parameters and ORTEP diagrams for **1**−**5** (50 pages). Ordering information is given on any current masthead page.

IC970844S

(28) Hotzelmann, R.; Wieghardt, K.; Florke, U.; Haupt, H. J.; Weatherburn, D. C.; Bonvoisin, J.; Blondin, G.; Girerd, J. J. *J. Am. Chem. Soc.* **1992**, *114*, 1681.